Experimental evaluation of the influence of scattered radiation on quantitative spectral CT imaging

Artur Sossin*[a], Michal Rokni[b], Bernhard Brendel[a], Heiner Daerr[a], Axel Thran[a], Klaus Erhard[a]

[a] Philips Research, Röntgenstrasse 24–26, 22335 Hamburg, Germany
[b] Philips Healthcare, Global Advanced Technologies, CT, Haifa, Israel

ABSTRACT

With the emergence of energy-resolved x-ray photon counting detectors multi-material spectral x-ray imaging has been made possible. This form of imaging allows the discrimination and quantification of individual materials comprising an inspected anatomical area. However, the acquisition of quantitative material data puts strong requirements on the performance capabilities of a given x-ray system. Scattered radiation is one of the key sources of influencing the quality of material quantification accuracy. The aim of the present investigation was to assess the impact of x-ray scatter on quantitative spectral CT imaging using a pre-clinical photon counting scanner prototype. Acquisitions of a cylindrical phantom with and without scatter were performed. The phantom contained iodine and gadolinium inserts placed at various locations. The projection data was then decomposed onto a water-iodine-gadolinium material basis and reconstructed. An analysis of the resulting iodine and gadolinium material images with and without scatter was conducted. It was concluded that, at an SPR level of up to 3.5%, scatter does not compromise material quantification for all investigated gadolinium concentrations, but for iodine a substantial underestimation was observed. The findings in this study suggest that scatter has a lower impact on K-edge material imaging in comparison with material imaging not featuring a K-edge.

Keywords: spectral photon counting CT, scattered radiation, contrast material quantification

1. INTRODUCTION

The extensive research and development of x-ray detector technologies has led to the advent of new types of sensors capable of x-ray photon counting and energy discrimination at flux rates employed in the respective imaging modalities. With the aid of such detectors multi-material spectral x-ray imaging has been made possible. This form of imaging allows the acquisition of additional diagnostic information during medical x-ray examinations. More precisely, individual materials (e.g. bone, muscle tissue, fat, contrast agent, etc.) comprising an inspected anatomical region can be discriminated and their amount quantified. However, the acquisition of quantitative material data puts strong requirements on the performance capabilities of a given x-ray system. Scattered radiation[1–6], limited photon statistics[7], pile-up and detector short comings can all have a substantial impact on the accuracy of spectral imaging data. In order to support the development of mitigation strategies for the aforementioned issues a thorough analysis of their influence on quantitative spectral imaging is required.

In the case of x-ray scatter, several simulated studies evaluating its impact on both spectral radiography[5] and computed tomography (CT)[3,4,6] have been conducted. However, such investigations can prove to be limited due to incomplete modelling of the imperfections of a real photon counting x-ray system. In the present study the authors aim at assessing the impact of x-ray scatter on quantitative spectral CT imaging with a pre-clinical photon counting scanner prototype.

The remaining part of the paper consists of three sections. In section 2 the spectral CT prototype employed in the measurements is described alongside with the geometrical configuration and phantom. Additionally, scattered radiation measurements are discussed. Results are then presented in section 3 accompanied by the corresponding discussion. The paper is concluded in section 4.

2. MEASUREMENT SET-UP

For the evaluation of the impact of scattered radiation on material quantification in spectral CT, several phantom acquisitions were performed on a prototype pre-clinical system. The CT scanner is based on a clinical Philips iCT gantry with the conventional scintillator detector replaced by an energy-resolved photon-counting CdZnTe detector of smaller

Medical Imaging 2018: Physics of Medical Imaging, edited by Joseph Y. Lo, Taly Gilat Schmidt, Guang-Hong Chen, Proc. of SPIE Vol. 10573, 105731B
© 2018 SPIE · CCC code: 1605-7422/18/$18 · doi: 10.1117/12.2293476

Downloaded From: https://www.spiedigitallibrary.org/conference-proceedings-of-spie on 7/10/2018
Terms of Use: https://www.spiedigitallibrary.org/terms-of-use

coverage (Figure 1). The detector consists of 32×616 pixels (500 μm pixel size) with 5 energy-channels (bins) employing Philips' proprietary ChromAIX2 application-specific integrated circuit[8]. Only 9 rows of the image sensor were read out. Consequently, the collimation was adjusted to 9 rows leading to an effective z-collimation of around 2.5 mm in the scanner iso-center. The system was operated without an anti-scatter grid (ASG). The imaging field-of-view (FOV) attainable by the respective system is 17 cm. The tube settings of the prototype scanner were configured to 50 mA with a 1 s acquisition time and 120 kVp. The 50 mA configuration was chosen in order to best avoid both the influence of pile-up and low-counts on material quantification.

Figure 1. Prototype pre-clinical photon counting x-ray CT system used for measurements.

The acquisitions featured a 13 cm cylindrical Delrin phantom with iodine and gadolinium solution inserts (1 cm diameter) placed at the iso-center of the scanner (Figure 2). A total of 4 inserts with different concentrations was considered for each material. The iodine concentrations were 0 mg/ml, 1.0±0.1 mg/ml, 4.3±0.4 mg/ml and 7.0±0.7 mg/ml. For gadolinium the values were 0 mg/ml, 1.0±0.1 mg/ml, 3.9±0.2 mg/ml and 15.7±0.6 mg/ml. Two types of CT scans were performed. In the first one the inserts of iodine/gadolinium were placed in the inner/outer part of the object (as marked in Figure 2) whilst in the second Iodine inserts were put in place of the ones with gadolinium and vice versa. The aim was to consider various local scatter levels. Additionally, for each type of acquisition, two realizations were performed to further reduce image noise.

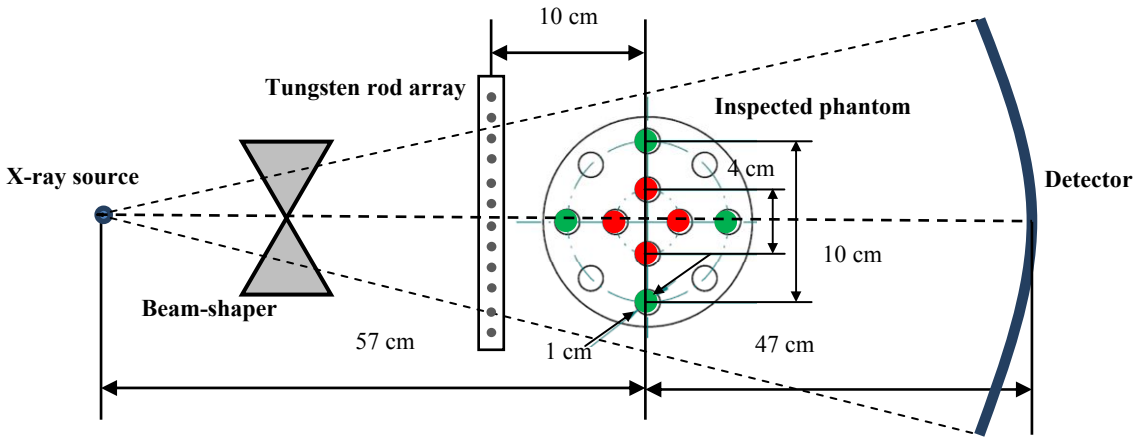

Figure 2. The geometric configuration of the conducted experiments. Phantom inserts comprising iodine and gadolinium are marked with red and green respectively.

Downloaded From: https://www.spiedigitallibrary.org/conference-proceedings-of-spie on 7/10/2018
Terms of Use: https://www.spiedigitallibrary.org/terms-of-use

In order to obtain information on the scattered radiation in both types of scans, the well-known beam-stop method was used[9]. To do this, a supplemental projection acquisition of the phantom with the same settings as were used for the iodine-gadolinium scans was performed. However, an array of tungsten rods was added to the system between the object and the x-ray source (Figure 2). A total of 24 rods with a 3 mm diameter and 4 cm height was used. The spacing between each one was 6 mm. The elements of the array allowed the acquisition of scattered radiation in selected regions of the detector corresponding to the projections of the rod centers. In these areas, primary radiation was completely blocked and only scatter remained. Note that off-focal radiation can also contribute to the scattered radiation measured with the current configuration. From these sparse scatter samples a full scatter signal profile on the detector was obtained by cubic spline interpolation. Since the investigated phantom was a cylinder centered at the iso-center of the system and was practically homogeneous, the assumption of a scatter distribution invariant of projection was made. Finally, an estimation of scatter free projection data of both types of iodine-gadolinium scans was obtained by subtracting the acquired scatter profile from each projection in the respective datasets.

Having obtained projection data of the phantom with and without scatter, a maximum-likelihood based basis material decomposition[10] of each dataset was performed. A water-iodine-gadolinium basis was used. The decomposed data was then reconstructed with the aid of a filtered back-projection algorithm. In order to reduce the impact of image noise on the present assessment, the resulting images were averaged in slice direction as well as among the two realizations considered for each dataset.

The analysis was based on iodine and gadolinium images obtained from the datasets with and without scatter, respectively. More precisely, for each insert i of material m, the average absolute ($a(m,i)$) and relative ($r(m,i)$) difference between the concentration values obtained with and without the presence of scatter was computed:

$$a(m,i) = \frac{1}{K}\sum_{p\in k}[c(m,i,p) - c_{sc}(m,i,p)] \tag{1}$$

and

$$r(m,i) = \frac{a(m,i)}{c_{True}(m,i)}. \tag{2}$$

In (1) $c(m,i,p)$ and $c_{sc}(m,i,p)$ denote the concentration of material m in insert i and image pixel p measured without and with scatter correction, respectively. Additionally, k denotes the circular region of interest (ROI) placed on the insert of interest and comprising K image pixels. The quantity $c_{True}(m,i)$ in (2) reflects the true concentration of a given material m in insert i. Finally, for the differences provided in (1) and (2), uncertainties were also computed via the following formulae:

$$\Delta a(m,i) = \sqrt{\frac{1}{K(K-1)}\sum_{p\in k}\left([c(m,i,p) - c_{sc}(m,i,p)] - \frac{1}{K}\sum_{p\in k}[c(m,i,p) - c_{sc}(m,i,p)]\right)^2} \tag{3}$$

and

$$\Delta r(m,i) = \sqrt{\left(\frac{\Delta a(m,i)}{c_{True}(m,i)}\right)^2 + \left(\frac{\Delta a(m,i)\Delta c_{True}(m,i)}{\left(c_{True}(m,i)\right)^2}\right)^2}. \tag{4}$$

The quantity $\Delta a(m,i)$ in (3) and $\Delta r(m,i)$ in (4) denotes the uncertainty of the absolute ($a(m,i)$) and relative ($r(m,i)$) concentration changes, respectively.

3. RESULTS

Firstly, iodine (Figure 3) and gadolinium (Figure 4) basis images reconstructed from the scatter corrected data are p-rovided to illustrate the decomposition results, insert placement and ROI regions used for concentration difference calculation. The total photon count scatter-to-primary ratio (SPR) for the inner inserts varied between 3.0% and 3.5% among projections of the CT scan whilst for the outer inserts this value was between 2.2% and 3.5%, respectively. The

Downloaded From: https://www.spiedigitallibrary.org/conference-proceedings-of-spie on 7/10/2018
Terms of Use: https://www.spiedigitallibrary.org/terms-of-use

variation of SPR per bin for the inner and outer inserts was 1.7–3.5% and 1.2–3.5%, respectively. The lowest and highest SPRs per bin correspond to the high- and low-energy bin, respectively.

Iodine concentration images, mg/ml

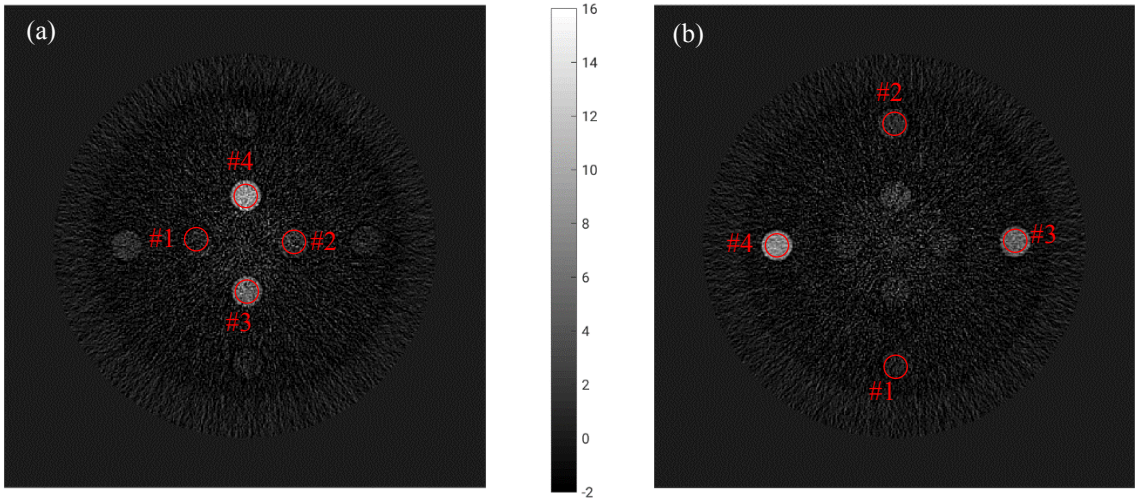

Figure 3. Iodine concentration images with the inner (a) and outer (b) positioning of the respective material inserts. Red circles mark the ROIs used for concentration difference estimation. ROI regions #1, #2, #3 and #4 correspond to 0 mg/ml, 1.0±0.1 mg/ml, 4.3±0.4 mg/ml and 7.0±0.7 mg/ml concentration inserts, respectively.

Gadolinium concentration images, mg/ml

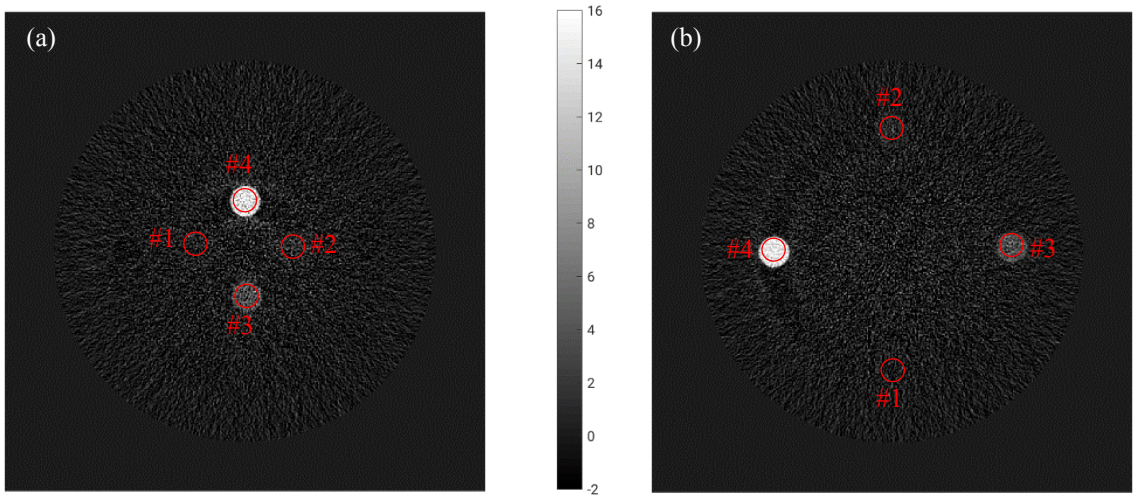

Figure 4. Gadolinium concentration images with the inner (a) and outer (b) positioning of the respective material inserts. Red circles mark the ROIs used for concentration difference estimation. ROIs #1, #2, #3 and #4 correspond to 0 mg/ml, 1.0±0.1 mg/ml, 3.9±0.2 mg/ml and 15.7±0.6 mg/ml concentration inserts, respectively.

Based on the ROI data acquired from various material inserts (Figure 3 and Figure 4) with and without scatter correction, absolute concentration differences along with associated uncertainties were computed via (1) and (3), respectively. The results are summarized in Table 1. Additionally, corresponding relative concentration changes with their uncertainties were obtained with the aid of (2) and (4), respectively.

Downloaded From: https://www.spiedigitallibrary.org/conference-proceedings-of-spie on 7/10/2018
Terms of Use: https://www.spiedigitallibrary.org/terms-of-use

Table 1. Absolute concentration changes (in mg/ml) for iodine and gadolinium contrast agents due the presence of scatter for both outer and inner insert position acquisitions.

Material (position) / ROI	#1	#2	#3	#4
Iodine (inner)	-0.26±0.03	-0.25±0.04	-0.44±0.04	-0.49±0.05
Iodine (outer)	-0.18±0.02	-0.16±0.02	-0.20±0.02	-0.29±0.03
Gadolinium (inner)	0.04±0.03	0.01±0.03	-0.08±0.03	-0.01±0.03
Gadolinium (outer)	-0.08±0.02	-0.00±0.02	0.01±0.02	-0.01±0.02

Table 2. Relative concentration changes for iodine and gadolinium contrast agents due to the presence of scatter for both outer and inner insert position acquisitions.

Material (position) / ROI	#2	#3	#4
Iodine (inner)	-25%±4%	-10%±1%	-7%±1%
Iodine (outer)	-16%±3%	-4.6%±0.7%	-4.2%±0.6%
Gadolinium (inner)	1%±3%	-2.1%±0.8%	-0.1%±0.2%
Gadolinium (outer)	-0%±2%	0.2%±0.5%	-0.1%±0.1%

From both Table 1 and Table 2 one notes that, at the investigated total photon count SPR levels of up to 3.5%, scatter contributes to an underestimation of iodine concentrations and has no substantial effect on gadolinium concentrations within the uncertainty of the present evaluation. The range of absolute and relative concentration change due to scatter recorded for iodine was -0.49–-0.16 mg/ml and -25%–-4.2%, respectively. Generally, the underestimation of contrast agent concentrations is expected as scattered radiation contributes to an increase in x-ray signal recorded by the pixels, which is equivalent to having less attenuating material (lower contrast agent concentration). Furthermore, scatter also alters the energy-distribution of the x-ray signal measured by the detector due to the scatter spectrum being shifted towards lower photon energies (Compton interactions) as compared to the primary one.

The absence of scatter influence on gadolinium concentrations can be linked to the corresponding material having its attenuation K-edge in the x-ray energy interval measured by the detector. This in turn creates a strong spectral feature that is not easily compromised by the presence of an additional scatter signal.

Another important point is that when comparing the inner and outer iodine insert configuration from Table 1 and Table 2, one can observe that the concentration changes for all inserts are lower for the outer insert configuration. This is directly related to a decreased amount of scatter in projection regions corresponding to the outer parts of the phantom (total photon count SPR of 3.0%–3.5%) compared to the inner ones (total photon count SPR of 2.2%–3.5%).

Overall, one can state that, given an acceptance criteria of 10%, the current system performs well under the influence of scatter for all gadolinium concentrations and for iodine concentrations greater than or equal to 4.3 mg/ml. However, in clinical practice, iodine concentrations in the interval of 1.0–4.0 mg/ml are usually of interest. The underestimation of iodine in this concentration region reached up to -25% for a 1.0 mg/ml concentration. Thus, it can be stated that scatter can strongly influence quantification accuracy in clinical practice. Note that the pre-clinical CT scanner features only a small FOV and z-coverage. For clinical use, a larger FOV and z-coverage is required. This would entail much higher scatter levels and thus lead to even higher iodine concentration changes than observed in the present study. Although, this can be partially compensated for by employed hardware such as an ASG as well as by the means of software-based

Downloaded From: https://www.spiedigitallibrary.org/conference-proceedings-of-spie on 7/10/2018
Terms of Use: https://www.spiedigitallibrary.org/terms-of-use

correction measures, the efficiency of such techniques is required to be considerably higher for spectral photon-counting than for conventional CT.

4. CONCLUSION

The evaluation of the impact of scattered radiation on iodine and gadolinium quantification in spectral CT imaging showed a high concentration change for iodine due to scattered radiation. More precisely, an absolute change between -0.49 mg/ml (7.0 mg/ml concentration) and -0.16 mg/ml (1.0 mg/ml concentration) was observed for the respective material. Gadolinium was practically unaffected with scatter induced concentration changes remaining, in almost all cases, within the uncertainty limits of the respective values. It was concluded that scatter does not compromise material quantification on the current system for all gadolinium concentrations, but for iodine a substantial underestimation was observed. The findings in this study suggest that scatter has a much lower impact on K-edge imaging in comparison with material imaging not featuring a K-edge.

ACKNOWLEDGEMENTS

The authors are very grateful to Yoad Yagil, Mark Limkeman, Amir Livne, Ira Blevis, David Braunstein, Elias Lahoud, Gilad Shechter and Younes Yaron from Philips' CT business in Haifa, Israel for their constant support of the authors' work and valuable comments and discussions.

REFERENCES

[1] Rührnschopf, E.P. and Klingenbeck, K., "A general framework and review of scatter correction methods in x-ray cone-beam computerized tomography. Part 1: Scatter compensation approaches," Med. Phys. 38(7), 4296–311 (2011)

[2] Rührnschopf, E.P. and Klingenbeck, K., "A general framework and review of scatter correction methods in x-ray cone-beam computerized tomography. A general framework and review of scatter correction methods in cone beam CT. Part 2: scatter estimation approaches," Med. Phys. 38(9), 5186–99 (2011)

[3] Wiegert, J., Engel, K. J. and Herrmann C., "Impact of scattered radiation on spectral CT," Proc. of SPIE 7258, 72583X (2009).

[4] Schmidt, T.G., "CT energy weighting in the presence of scatter and limited energy resolution," Med. Phys. 37(3), 1056–67 (2010).

[5] Sossin, A., Rebuffel, V., Tabary, J., Létang, J. M., Freud, N. and Verger, L., "Influence of Scattering on Material Quantification Using Multi-Energy X-ray Imaging," Proc. of IEEE NSS/MIC, 1–5 (2014).

[6] Lu, Y., Peng, B., Lau, B.A., Hu, Y.H., Scaduto, D.A., Zhao, W. and Gindi, G., "A scatter correction method for contrast-enhanced dual-energy digital breast tomosynthesis," Phys. Med. Biol. 60(16), 6323–54 (2015).

[7] Lee, O., Kappler, S., Polster, C. and Taguchi, K., "Estimation of basis line-integrals in a spectral distortion-modeled photon counting detector using low-order polynomial approximation of x-ray transmittance," IEEE Trans. Med. Imaging 36(2), 560–573 (2016).

[8] Steadman, R., Herrmann, C. and Livne, A., "ChromAIX2: A large area, high count-rate energy-resolving photon counting ASIC for a Spectral CT Prototype," Nucl. Instr. Meth. Phys. Res. Sec. A 862, 18–24 (2017).

[9] Peterzol, A., Létang, J. M. and Babot, D., "A beam stop based correction procedure for high spatial frequency scatter in industrial cone-beam X-ray CT," Nucl. Instr. Meth. Phys. Res. Sec. B 26(18), 4042–54 (2015).

[10] Roessl, E. and Proksa, R., "K-edge imaging in x-ray computed tomography using multi-bin photon counting detectors," Phys. Med. Biol. 52(15), 4679–96 (2007).

Downloaded From: https://www.spiedigitallibrary.org/conference-proceedings-of-spie on 7/10/2018
Terms of Use: https://www.spiedigitallibrary.org/terms-of-use